| | |
|---|---|
| Title | The statistics of gamma-ray pulsars |
| Author(s) | Cheng, KS; Zhang, L |
| Citation | Astrophysical Journal Letters, 1998, v. 498 n. 1 PART I, p. 327-341 |
| Issued Date | 1998 |
| URL | http://hdl.handle.net/10722/43221 |
| Rights | Creative Commons: Attribution 3.0 Hong Kong License |

THE ASTROPHYSICAL JOURNAL, 498:327–341, 1998 May 1


# THE STATISTICS OF GAMMA-RAY PULSARS

K. S. CHENG AND L. ZHANG
Department of Physics, University of Hong Kong, Pokfulam Road, Hong Kong; hrspksc@hkucc.hku.hk, ZhangL@hkuphy1.hku.hk
*Received 1997 July 15; accepted 1997 December 9*

## ABSTRACT

We use Monte Carlo methods to simulate the properties of a Galactic population of rotation-powered pulsars in the self-consistent outer gap model proposed by Zhang & Cheng, where the initial magnetic field and spatial and velocity distributions of the neutron stars at birth are obtained from the statistical results of radio pulsars. We obtain the distance, period, age, magnetic field, and $\gamma$-ray flux distributions of the $\gamma$-ray pulsars whose $\gamma$-ray and radio fluxes are above the detectable threshold fluxes. Furthermore, we simulate the properties of Geminga-like pulsars and obtain the possible parametric region and the number of the Geminga-like pulsars. In our simulations, the different beaming effects of radio and $\gamma$-ray beams are taken into account. We predict that there may be $\sim 11$ $\gamma$-ray pulsars that are detectable at both radio and $\gamma$-ray energies and $\sim 37$ Geminga-like pulsars in the Galactic plane ($|b| < 5°$) if the $\gamma$-ray beaming fraction is 0.67 and the birthrate of the neutron stars is 1 per century. Compared to the flux distribution, individual spectrum, and distance distribution obtained by assuming OB star associations of our simulated Geminga-like pulsars and the unidentified EGRET sources at $|b| < 5°$, we conclude that the majority of the unidentified $\gamma$-ray point sources near the Galactic plane may be Geminga-like pulsars. We also suggest that the most possible radio pulsars likely to be confirmed as $\gamma$-ray pulsars in future are those with $L_X/\dot{E}_{sd} \sim 10^{-3}$.

*Subject headings:* gamma rays: theory — pulsars: general — stars: neutron — stars: statistics

## 1. INTRODUCTION

A database of 706 radio pulsars can be obtained from the archive data of Princeton University (also see Taylor, Manchester, & Lyne 1993). Furthermore, the upper limits on pulsed $\gamma$-ray emission for 350 pulsars have been given (Nel et al. 1996), which include two kinds of pulsars: canonical pulsars and millisecond pulsars. Of these pulsars, only six have been confirmed to emit high-energy $\gamma$-rays in the energy range of EGRET (PSR B1509−58 was detected up to $\sim 1$ MeV but has not been detected by EGRET). Ramanamurthy et al. (1996) have reported possible evidence for pulsed $\gamma$-ray emission above 50 MeV from PSR B0656+14. In addition, Geminga was not detected as a radio pulsar. This information allows us to perform useful statistical studies of the observed $\gamma$-ray pulsar parameters, such as the distance, period, age, magnetic field, and $\gamma$-ray flux distributions and may also provide clues about how to predict possible candidates for $\gamma$-ray pulsars. In fact, based on the data observed by EGRET, many authors have already made some predictions of possible candidates for $\gamma$-ray pulsars (e.g., Cheng & Ding 1994; Brazier et al. 1994; Thompson et al. 1994; Fierro et al. 1995). In particular, Cheng & Ding (1994) predicted that PSR B1951+32 should be the pulsar confirmed to be a $\gamma$-ray pulsar after PSR B1055−52. Fierro (1995) also pointed out that pulsars PSR J0034−0534, J0613−0200, PSR B1046−58, B1832−06, and B1853+01 are the most probable candidates for $\gamma$-ray pulsars. This information can also be used to test the validity of the various $\gamma$-ray pulsar models. Moreover, the second EGRET catalog and its supplement (Thompson et al. 1995, 1996) lists 96 unidentified point sources, where 30 unidentified point sources are in low Galactic latitudes ($|b| < 5°$). It is believed that the unidentified point sources at the Galactic plane probably consist of young pulsars (e.g., Kaaret & Cottam 1996; Yadigaroglu & Romani 1997). We will use these observation data to compare with our analysis. Generally, $\gamma$-ray models can be divided into polar gap and outer gap models. In polar gap models, charged particles are accelerated in charge-depleted zones near the pulsar's polar cap and $\gamma$-rays are produced through curvature-radiation–induced $\gamma$-$B$ pair cascade (e.g., Harding 1981) or through Compton-induced pair cascades (Dermer & Sturner 1994). In the outer gap models, large regions of the magnetospheric charge depletion (gaps) are assumed to result from a global current flow pattern through the magnetosphere, and charged particles that are likely electrons/positrons are accelerated to extreme relativistic energies because of large electric fields along the magnetic lines in these gaps. The observed $\gamma$-rays are produced by the synchrotron radiation (Vela type) and synchrotron self-Compton mechanism (Crab type) of secondary $e^{\pm}$ pairs (Cheng, Ho, & Ruderman 1986a, 1986b, hereafter respectively CHR I, CHR II; Ho 1989; Chiang & Romani 1992; Cheng & Ding 1994; Cheng & Wei 1995; Romani 1996) or by synchro-curvature radiation of primary $e^{\pm}$ pairs (Zhang & Cheng 1997, hereafter ZC97). Based on known $\gamma$-ray pulsars, studies have been made of the luminosity and conversion efficiency of $\gamma$-rays in various models. Harding (1981) predicted that the $\gamma$-ray luminosity from a pulsar can be expressed by $L_\gamma^{th}(>100$ MeV$) \approx 1.2 \times 10^{35} B_{12}^{0.95} P^{-1.7}$ photons s$^{-1}$, where $B_{12}$ is the magnetic field in units of $10^{12}$ G and $P$ is the pulsar period in seconds. Dermer & Sturner (1994) predicted that the $\gamma$-ray luminosity from the polar cap is given by $L_\gamma^{th} \approx 10^{32} B_{12}^{3/2} P^{-2}$ ergs s$^{-1}$. Comparing the observed $\gamma$-ray luminosities (or upper limits) with those predicted by the models of Harding (1981) and Dermer & Sturner (1994), Nel et al. (1996) suggested that both polar gap models overestimate $L_\gamma$ at high luminosity and underestimate $L_\gamma$ at low luminosity. A recent phenomenological polar gap model (Rudak & Dyks 1997) can give a more satisfactory explanation for $L_\gamma$ from pulsars. For the outer gap models, the predicted $\gamma$-ray luminosity depends on the solid angle of $\gamma$-ray beaming. Yadigaroglu & Romani (1995) suggested that the conversion efficiency of $\gamma$-rays ($\eta_\gamma \equiv L_\gamma/\dot{E}_{sd}$, where $\dot{E}_{sd}$ is the

spin-down power) should increase with pulsar age to derive a phenomenological scaling law of the form $\eta_\gamma = 3.2 \times 10^{-5}\tau^{0.76}$, where $\tau$ is the pulsar age in units of years. Recently we have proposed a new self-consistent outer gap model, called the thick outer gap model, to describe the high-energy $\gamma$-ray radiations from mature pulsars (ZC97). In this paper, we will use the ZC97 model to determine general formulae for $\gamma$-ray flux and the luminosity and conversion efficiency of $\gamma$-rays from canonical pulsars that are functions of pulsar parameters, e.g., period and magnetic field strength. Using as a basis models for $\gamma$-ray production from pulsars, many authors have studied detailed statistical properties of $\gamma$-ray pulsars by using Monte Carlo methods. For example, Bailes & Kniffen (1992) investigated the polar gap model (Harding 1981) and outer gap model (CHR I, CHR II) to explain the Galactic diffuse $\gamma$-rays. Yadigaroglu & Romani (1995) have considered the properties of $\gamma$-ray pulsars in their outer gap model. Sturner & Dermer (1996) simulated the properties of the Galactic population of rotation-powered pulsars on the basis of their model for $\gamma$-ray production from pulsars. Here we will present the statistical analysis of $\gamma$-ray properties of rotation-powered pulsars based on our model. In § 2 we will review our outer gap model results and use the database (including only those pulsars with upper limits) given by Nel et al. (1996) to test our model. In § 3 we describe the Monte Carlo simulation of the Galactic pulsar population and present the simulation results. In § 4 we simulate the population of Geminga-like pulsars and compare that with the unidentified point sources of EGRET. In § 5 we further analyze the database of radio pulsars and give some predictions about the most possible candidates for $\gamma$-ray pulsars based on our model. Finally, a brief conclusion and discussion will be given in § 6.

## 2. REVIEW OF THE THICK OUTER GAP MODEL AND COMPARISON WITH THE OBSERVED DATA

We have proposed a self-consistent model of a thick outer gap to describe the high-energy $\gamma$-ray emission from mature pulsars (ZC97). In our model, the characteristic photon energy $E_\gamma(f)$ is completely determined by the size of the outer gap ($f$), which is the ratio between the outer gap volume and $R_L^3$, where $R_L$ is the light cylinder radius. Half of the primary $e^\pm$ pairs in the outer gap will move toward the star and lose their energy via the curvature radiation. The return particle flux can be approximated by $\dot{N}_{e^\pm} \approx \frac{1}{2} f \dot{N}_{\rm GJ}$, where $f$ is the fractional size of the outer gap and $\dot{N}_{\rm GJ}$ is the Goldreich-Julian particle flux (Goldreich & Julian 1969). Although most of the energy of the primary particles will be lost on the way to the star via curvature radiation, about $10.6P^{1/3}$ ergs per particle will still remain and will be finally deposited on the stellar surface. This is because the curvature radiation loss depends on the 4th power of the Lorentz factor of the charged particles. When the Lorentz factor is below $\sim 10^7$, the timescale for the curvature energy loss will be longer than the time needed for the particle traveling to the star. This energy will then be emitted in the form of X-rays from the stellar surface (such a process has been described by Halpern & Ruderman 1993). The characteristic energy of X-rays is given by $E_{\rm X}^h \approx 3kT \approx 1.2 \times 10^3 f^{1/4} P^{-1/6} B_{12}^{1/4}$ eV, where $P$ is the pulsar period in units of seconds, $B_{12}$ is the dipolar magnetic field in units of $10^{12}$ G and the radius of the neutron star is assumed to be $10^6$ cm. Furthermore, the keV X-rays from a hot polar cap will be reflected back to the stellar surface due to the cyclotron resonance scattering if there is a large density of magnetically produced $e^\pm$ pairs near the neutron star surface (Halpern & Ruderman 1993), and will eventually reemit softer thermal X-rays with characteristic temperature (ZC97)

$$T_s \approx 3.8 \times 10^5 f^{1/4} P^{-5/12} B_{12}^{1/4} R_6 \ {\rm K} \quad (1)$$

and power

$$L_{\rm X}^{\rm soft} \approx 1.4 \times 10^{31} f B_{12} P^{-5/3} \ {\rm ergs\ s^{-1}} . \quad (2)$$

Calculations show that the optical depth of the soft X-ray photons in the outer gap is only $\sim L_{\rm X}^{\rm soft} \sigma_{{\rm X}\gamma \to e^\pm} / 4\pi r k T c \sim 10^{-4}$. However, since the potential drop of the outer gap is $\sim 10^{15}$ V (CHR I, CHR II), each primary $e^+/e^-$ passing through the gap can emit more than $10^5$ multi-GeV curvature photons. Such huge multiplicity can produce a sufficient number of $e^\pm$ pairs to sustain the gap as long as the center-of-mass energy of X-ray and curvature photonsis higher than the threshold energy of the electron/positron pair production, i.e., $E_{\rm X} E_\gamma \geq (m_e c^2)^2$. From the condition for the photon-photon pair production, the fractional size of the outer gap limited by the soft thermal X-rays from the neutron star surface can be determined as

$$f = 5.5 P^{26/21} B_{12}^{-4/7} . \quad (3)$$

It should be emphasized that $f \leq 1$ and any fluctuation of the gap can be stabilized by the processes described above. In fact, the increase in gap size will increase the X-ray flux and the overproduced pairs can reduce the gap size. Similarly, a decrease in the gap size will produce insufficient pairs and result in an increase in the gap size. Furthermore, it has been argued (Halpern & Ruderman 1993; ZC97) that the primary electrons/positrons leaving the outer gap emit curvature photons, which will be converted into the secondary $e^\pm$ pairs by the neutron star magnetic field if these photons come close to the star, where the pair production condition in strong magnetic field is satisfied (Erber 1966; Ruderman & Sutherland 1975). In ZC97 we have estimated that the magnetic pair production will start at about 10–20 stellar radii. Since the primary photon energies are of the order of a few GeV for all known $\gamma$-ray pulsars, the synchrotron photons will have a typical energy of the order of a few hundred MeV. Most of these synchrotron photons are moving toward the star because the local field lines are converging toward the star. Cheng, Gil, & Zhang (1998) estimated that when these photons move in toward the star by a factor of 0.37, the local magnetic field will become strong enough to convert these synchrotron photons to pairs which subsequently lose their energies via synchrotron radiation with a characteristic synchrotron energy of the order of a few tens of MeV. These processes can repeat at least once more before the synchrotron photon energy reduces to $\sim$MeV and the spectral index steepens from $\sim -1.5$ to $\sim -2$. They estimated that the luminosity of this nonthermal X-ray component is

$$L_{\rm X}^{\rm syn} \approx 8.8 \times 10^{-6} (\tan^4 \chi) f^{1/2} B_{12}^{5/12} P^{-17/12} L_{\rm sd} , \quad (4)$$

where $\chi$ is the inclination angle between the magnetic axis and the rotation axis. Cheng et al. (1998) have pointed out that $L_{\rm X}/\dot{E}_{\rm sd} \sim 10^{-3}$ for pulsars with $f \leq 1$ and $\chi \sim 55°$, and this result seems quite consistent with the observed data (Becker & Trümper 1997). We want to point out that X-ray

luminosity is predicted by the outer gap model, and it plays an important role in our later analysis for identifying which unidentified EGRET sources and radio pulsars are possible $\gamma$-ray pulsars. The predicted X-ray photon spectra for $E_X \leq 1$ MeV are given by

$$\frac{d\dot{N}_X}{dE_X} = F_{bb}(T_s, E_X) + AE_X^{-2}, \quad (5)$$

where $F_{bb}$ is the blackbody spectrum with a characteristic temperature $kT_s = E_X^s$, which satisfies

$$\int F_{bb} E_X \, dE_X = L_X^{soft}, \quad (6)$$

and

$$A \approx 1.7 \times 10^{35} f^{1/2} P^{-65/12} B_{12}^{29/12} \frac{\tan^4 \chi}{\ln\{\text{MeV}/[\hbar eB(r)/mc]\}}, \quad (7)$$

where $r$ is the distance to the star at which the magnetic field becomes strong enough to convert the curvature photons into pairs. Here we would like to remark that our thick outer gap model does not work very well for very young pulsars, e.g., the Crab pulsar, because we have ignored the Compton cooling of the return current. In very young pulsars, the surface temperature is determined by cooling instead of polar cap heating and is sufficiently high that the inverse Compton scattering by the surface soft X-ray photons can reduce the energy of the return current (CHR II). ZC97 have also shown that the Lorentz factor of accelerated particles inside the outer gap is given by

$$\gamma(x) \approx 2 \times 10^7 f^{1/2} B_{12}^{1/2} P^{-1/4} x^{-3/4}, \quad (8)$$

where $x = s/R_L$, $s$ is the curvature radius, and $R_L$ is the radius of the light cylinder. The energy distribution of the accelerated particles is given by

$$\frac{dN}{dE_e} dE_e = \frac{dN}{dx} dx \approx 1.4 \times 10^{30} f B_{12} P^{-1} \left(\frac{x}{x_{max}}\right)^{9/4}, \quad (9)$$

where $E_e$ is the energy of the accelerated particles and $x_{max}$ is the maximum curvature radius of the magnetic field lines in units of the radius of the light cylinder. The radiation spectrum produced by the accelerated particles with a power-law distribution in the outer gap can be expressed as (Cheng & Zhang 1996; ZC97)

$$\frac{d^2N_\gamma}{dE_\gamma dt} \approx \frac{\dot{N}_0}{E_\gamma} \int_{x_{min}}^{x_{max}} x^{3/2} \frac{R_L}{r_c} \times \left[\left(1 + \frac{1}{r_c^2 Q_2^2}\right) F(y) - \left(1 - \frac{1}{r_c^2 Q_2^2}\right) y K_{2/3}\right] dx \quad (10)$$

with

$$\dot{N}_0 = \frac{\sqrt{3} e^2 \gamma_0 N_0}{2hR_L} \approx 6.2 \times 10^{37} \tau^{-11/56} X_{max}^{-9/4} \text{ s}^{-1}, \quad (11)$$

$$r_c = xR_L \Big/ \left[\left(1 + \frac{r_B}{R_L} \frac{1}{x}\right) \cos^2 \alpha + \frac{R_L}{r_B} x \sin^2 \alpha\right], \quad (12)$$

and

$$Q_2 = \frac{1}{xR_L} \left[\left(\frac{r_B}{R_L} \frac{1}{x} + 1 - 3 \frac{R_L}{r_B} x\right) \cos^4 \alpha + 3 \frac{R_L}{r_B} x \cos^2 \alpha + \left(\frac{R_L}{r_B}\right)^2 x^2 \sin^4 \alpha\right]^{1/2}, \quad (13)$$

where $r_B = \gamma mc^2 \sin \alpha / eB$; $\alpha$ is the pitch angle of a charged particle in the curved magnetic field ($B$) and $\alpha \approx 0.79 f^{1/2} B_{12}^{-3/4} P^{7/4} x^{17/4}$; $\tau$ is the pulsar's age in units of years; $F(y) = \int_y^\infty K_{5/3}(z) dz$; $K_{5/3}$ and $K_{2/3}$ are modified Bessel functions of order 5/3 and 2/3; and $y = E_\gamma / E_c$. The characteristic energy of the radiated photons is given by

$$E_c = \frac{3}{2} \hbar c \gamma(x)^3 Q_2 \approx 640.5 \left(\frac{P}{B_{12}}\right)^{3/28} x^{-13/4} (R_L x Q_2) \text{ MeV}. \quad (14)$$

Therefore, the integrated flux with $E_\gamma > 100$ MeV at the Earth is given by

$$F(E_\gamma > 100 \text{ MeV}) = \frac{1}{\Delta\Omega_\gamma d^2} \int_{100 \text{ MeV}}^{10 \text{ GeV}} \frac{d^2N_\gamma}{dE_\gamma dt} dE_\gamma, \quad (15)$$

where $\Delta\Omega_\gamma$ is the solid angle of $\gamma$-ray beaming and $d$ is the distance to the pulsar. In our model, there are three parameters, i.e., $\Delta\Omega_\gamma$, $x_{min}$ and $x_{max}$. These three parameters depend on the detailed structure of the outer gap and the inclination angle of the pulsar. We have calculated the differential flux of $\gamma$-rays for the known $\gamma$-ray pulsars and found $x_{max} \sim 2$, and $\Delta\Omega_\gamma$ and $x_{min}$ vary between 0.5 and 3.9 and between 0.55 and 0.7, respectively, for known $\gamma$-ray pulsars (ZC97). In Figure 1 we compare our model spectra from 0.1 keV to 10 GeV with the observed data. The dashed curve is the best-fit model curve with the fitting parameters shown in Table 1. The solid curve is the consistent fit in which we use one set of parameters for all $\gamma$-ray pulsars, i.e., $\Delta\Omega_\gamma = 2.0$, $x_{min} = 0.55$, and $x_{max} = 2.0$ for all $\gamma$-ray pulsars. We can see that the consistent-fit curves generally agree with the data quite well. In particular, the $\gamma$-ray flux above 100 MeV predicted by the consistent-fit curve agrees with the observed data to within a factor of 3. This set of consistent fitting parameters plays two very important roles in our later analysis. First, it allows us to predict the model $\gamma$-ray spectrum and flux for unidentified $\gamma$-ray sources if they are Geminga-like pulsars and radio pulsars. Second, in the outer gap model, radio and $\gamma$-rays do not in general come from the same place; we need to estimate the $\gamma$-ray beaming factor before we do our statistical analysis. In § 3.1 we will show how to estimate the $\gamma$-ray beaming factor from $\Delta\Omega_\gamma$. The energy flux of $\gamma$-rays between 100 MeV and 10 GeV can expressed as

$$S_\gamma^{th}(E_\gamma > 100 \text{ MeV}) = \frac{1}{\Delta\Omega_\gamma d^2} \int_{100 \text{ MeV}}^{10 \text{ GeV}} E_\gamma \frac{d^2N_\gamma}{dE_\gamma dt} dE_\gamma, \quad (16)$$

while the corresponding luminosity is

$$L_\gamma(E_\gamma > 100 \text{ MeV}) = \Delta\Omega_\gamma d^2 S_\gamma(E_\gamma > 100 \text{ MeV}). \quad (17)$$

We can calculate equation (17) numerically for given parameters of pulsars. Furthermore, the total $\gamma$-ray luminosity is given by (ZC97)

$$L_\gamma \approx 3.8 \times 10^{31} f^3 P^{-4} B_{12}^2 \text{ ergs s}^{-1}. \quad (18)$$

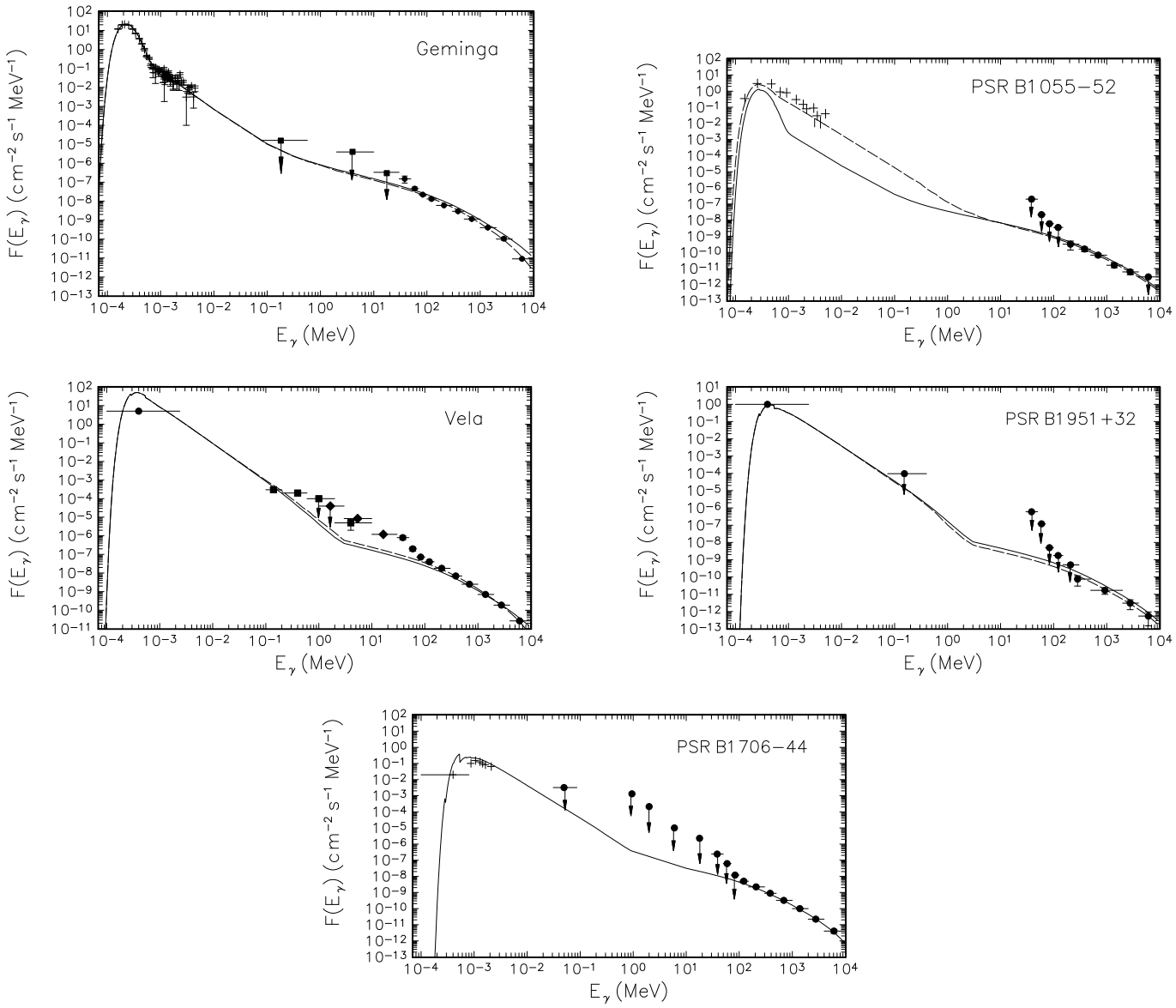


FIG. 1.—Comparisons of our model spectra from 0.1 keV to 10 GeV with the observed data for five known $\gamma$-ray pulsars detected by EGRET. The dashed curves are the best-fit model curves, and the solid curves are consistent-fit curves in which we use one set of parameters for all $\gamma$-ray pulsars.

From Figure 1 we can see that most of the $\gamma$-ray luminosity is contributed by $E_\gamma > 100$ MeV, so that the $\gamma$-ray luminosity with $E_\gamma > 100$ MeV can be approximated by equation (18). From equation (18), we can estimate the conversion efficiency of spin-down power into $\gamma$-rays. Using $\dot{E}_{\rm sd} \approx 3.8 \times 10^{31} P^{-4} B_{12}^2$ ergs s$^{-1}$, the conversion efficiency with $E_\gamma > 100$ MeV can be approximated by

$$\eta_\gamma(E_\gamma > 100 \text{ MeV}) \approx 10^{-4} \tau^{6/7} P^2 \ . \quad (19)$$

The comparisons between the theoretical integrated flux,

TABLE 1

BEST-FIT MODEL PARAMETERS[a] OF $\gamma$-RAY PULSARS

| Pulsar | $P$ (s) | $B_{12}$ (G) | $d$ (kpc) | $x_{\rm min}$[b] | $x_{\rm max}$[b] | $\Delta\Omega_\gamma$[b] | $\chi$[c] (deg) |
|---|---|---|---|---|---|---|---|
| Vela ..... | 0.089 | 3.4 | $0.5 \pm 0.1$ | 0.70 | 2.0 | 1.0 | 55.0 |
| B1951+32..... | 0.04 | 0.49 | $2.5^{+0.6}_{-1.0}$ | 0.55 | 2.0 | 2.4 | 55.0 |
| B1706−44..... | 0.102 | 3.1 | $1.82^{+0.7}_{-0.5}$ | 0.62 | 2.0 | 0.6 | 55.0 |
| Geminga..... | 0.237 | 1.6 | $0.25 \pm 0.1$ | 0.7 | 2.1 | 3.9 | 55.0 |
| B1055−52..... | 0.197 | 1.0 | $1.5 \pm 0.4$ | 0.55 | 2.1 | 2.6 | 77.0 |

[a] Values of the consistent-fit parameters are $x_{\rm min} = 0.55$, $x_{\rm max} = 2.0$, $\Delta\Omega = 2.0$, and $\chi = 55°$ for all $\gamma$-ray pulsars which are used for calculating the solid curves in Fig. 1.

[b] Values of the best-fit parameters for $\gamma$-rays.

[c] Values of the best-fit parameters for X-rays.

energy flux, luminosity, and conversion efficiency and the observed data of pulsars are presented in Zhang & Cheng (1998).

## 3. GALACTIC PULSAR POPULATION

In order to consider the luminosity and spatial evolution of a Galactic population of the canonical pulsars, the initial values of parameters of pulsars at birth, which include the initial position, velocity, period, and magnetic field strength, are needed. Furthermore, the beaming and selection effects at radio and $\gamma$-ray energies for the canonical pulsars have to be considered. In this section we will describe our Monte Carlo simulations of the Galactic pulsar population.

### 3.1. *Basic Parameters and Detectability of Pulsars*

The conventional assumption for the Galactic pulsar population is that pulsars are born at a rate (say $\sim 1/100$ yr) at spin periods of $P_0$, which vary exponentially with distance from the Galactic center and vary exponentially with distance from the Galactic plane. The birth location for each pulsar is estimated from spatial distributions in $z$ and $R$ (Paczyński 1990; Sturner & Dermer 1996), i.e.,

$$\rho_z(z) = \frac{1}{z_{\rm exp}}\, e^{-|z|/z_{\rm exp}}\,, \tag{20}$$

$$\rho_R(R) = \frac{a_R}{R_{\rm exp}^2}\, R e^{-R/R_{\rm exp}}\,, \tag{21}$$

where $z$ is the distance from the Galactic plane, $R$ is the distance from the Galactic center, $z_{\rm exp} = 75$ pc, $a_R = [1 - e^{-R_{\rm max}/R_{\rm exp}}(1 + R_{\rm max}/R_{\rm exp})]^{-1}$, $R_{\rm exp} = 4.5$ kpc, and $R_{\rm max} = 20$ kpc. The initial velocity of each pulsar is the vector sum of the circular rotation velocity at the birth location and a random velocity from the supernova explosion. The circular rotation velocity is determined by (Sturner & Dermer 1996)

$$v_{\rm circ} = \left[ R\left(\frac{d\Phi_{\rm sph}}{dR} + \frac{d\Phi_{\rm disk}}{dR} + \frac{d\Phi_{\rm halo}}{dR}\right)\right]^{1/2}, \tag{22}$$

where $\Phi_{\rm sph}$, $\Phi_{\rm disk}$, and $\Phi_{\rm halo}$ are spheroidal, disk, and halo components of Galactic gravitational potential, given by Paczyński (1990) as

$$\Phi_i(R, z) = \frac{GM_i}{\sqrt{R^2 + [a_i + (z^2 + b_i^2)^{1/2}]^2}}\,, \tag{23}$$

where $a_{\rm sph} = 0.0$ kpc, $b_{\rm sph} = 0.277$ kpc, and $M_{\rm sph} = 1.12 \times 10^{10}\, M_\odot$ for the spheroidal component, $a_{\rm disk} = 3.7$ kpc, $b_{\rm disk} = 0.200$ kpc, and $M_{\rm disk} = 8.07 \times 10^{10}\, M_\odot$ for the disk component. The halo component is given by

$$\Phi_{\rm halo}(r) = \frac{GM_{\rm halo}}{r_c}\left[\frac{1}{2}\ln\left(1 + \frac{r^2}{r_c^2}\right)^2 + \frac{r_c}{r}\arctan\left(\frac{r}{r_c}\right)\right], \tag{24}$$

where $r = (R^2 + z^2)^{1/2}$ is the distance to the Galactic center, $r_c = 6.0$ kpc, and $M_{\rm halo} = 5.00 \times 10^{10}\, M_\odot$. For the random velocity, their three-dimensional velocity distribution is accurately given by (Lyne & Lorimer 1994)

$$\rho_V(u) = \frac{4}{\pi}\,\frac{u}{(1 + u^4)}\,, \tag{25}$$

where $u = V/350$ km s$^{-1}$ and $V$ is the random velocity of the pulsar, which is chosen randomly and added to the circular velocity. The surface magnetic fields of the pulsars are distributed as a Gaussian in log $B$ with mean log $B_0 = 12.4$ and dispersion $\sigma_B = 0.3$, namely,

$$\rho_B(\log B) = \frac{1}{\sqrt{2\pi}\sigma_B}\exp\left[-\frac{1}{2}\left(\frac{\log B - \log B_0}{\sigma_B}\right)^2\right]. \tag{26}$$

Here we assume that the magnetic fields of pulsars do not decay. Furthermore, one of the pulsar parameters for Monte Carlo simulation is the initial period for each pulsar. Here we use the assumption that the initial rotation period distribution of the pulsars is a $\delta$-function at some period $P_0$ (Sturner & Dermer 1996). After giving the initial properties of a newly born pulsar, we can follow its trajectory and evolve its period until the present time. At any time $t$, the pulsar's location is determined by following its motion in the Galactic gravitational potential. Using the equations given by Paczyński (1990), the orbit integrations are performed using the fourth-order Runge-Kutta method with variable time step (Press et al. 1992) on the variables $R$, $V_R$, $z$, $V_z$, and $\phi$. Once the coordinates $[R(t), z(t), \phi]$ are determined, we can calculate the Galactic longitude and latitude and the distance of the pulsar, namely,

$$l = 57.^\circ3 \arcsin\left\{\frac{R(t)}{[R(t)^2 + R_\odot^2 - 2R(t)R_\odot\cos\phi]^{1/2}}\sin\phi\right\}, \tag{27}$$

$$b = 57.^\circ3 \arctan\left\{\frac{z(t)}{[R(t)^2 + R_\odot^2 - 2R(t)R_\odot\cos\phi]^{1/2}}\right\}, \tag{28}$$

and

$$d = \sqrt{[R(t)^2 + R_\odot^2 - 2R(t)R_\odot\cos\phi)]^{1/2} + z(t)^2}\,, \tag{29}$$

where $R_\odot = 8.0$ kpc is the Galactocentric distance of the Sun. Furthermore, the evolution of the pulsar's period can be represented by

$$P(t) = \left[P_0^2 + \left(\frac{16\pi^2 R_{\rm NS}^6 B^2}{3Ic^3}\right)t\right]^{1/2} \tag{30}$$

if the period evolution is due to the effects of magnetic dipole radiation, where $R_{\rm NS}$ is the neutron star radius, $I$ is the neutron star moment of inertia, and $c$ is the speed of light. The 400 MHz radio luminosity, $L_{400}$, of each model pulsar is determined from the following distribution (Narayan & Ostriker 1990):

$$\rho_{L_{400}}(P, \dot{P}) = 0.5\lambda^2 e^{-\lambda}\,, \tag{31}$$

where $\lambda = 3.6[\log(L_{400}/\langle L_{400}\rangle) + 1.8]$, $\log\langle L_{400}\rangle = 6.64 + \frac{1}{3}\log(\dot{P}/P^3)$, and $L_{400}$ is in units of mJy kpc$^2$. In order to generate a sample of detectable canonical pulsars, we need to consider the beaming effect of the radio beam. The radio beaming fraction can be expressed as (Emmering & Chevalier 1989)

$$f_r(\omega) = (1 - \cos\omega) + (\pi/2 - \omega)\sin\omega\,, \tag{32}$$

where a random distribution of magnetic inclination angles is assumed and $\omega$ is the half-angle of the radio emission cone. Earlier studies have assumed that $f_r \sim 0.2$ (i.e., $\theta \sim 10^\circ$) and $f_r$ is independent of pulsar period (e.g., Vivekanand & Narayan 1981). However, recent studies

indicate that $f_r$ depends on the pulsar period because the half-angle varies with period. Different models have different relations of half-angle and period (e.g., Narayan & Vivekanand 1983; Lyne & Manchester 1988; Biggs 1990; Gil, Kijak, & Seiradakis 1993; Gil & Han 1996). Here we will use the model of Lyne & Manchester (1988) corrected by Biggs (1990), i.e., $\omega = 6.^{\circ}2 \times P^{-1/2}$. Then, following Emmering & Chevalier (1989), a sample pulsar with a given period $P$ is chosen in one out of $f_r(P)^{-1}$ cases using the Monte Carlo method. For the $\gamma$-ray beaming effect, following the same consideration as the radio beaming effect given by Emmering & Chevalier (1989), the beaming fraction of the solid angle swept out by $\gamma$-ray pulsar beams is given by $f_\gamma = (1 - \cos\theta_\gamma) + (\pi/2 - \theta_\gamma)\sin\theta_\gamma$, where $\theta_\gamma$ is the half-angle of the $\gamma$-ray emission cone. Here we assume that the $\gamma$-ray beaming fraction is independent of the pulsar's period and use $\langle \Delta\Omega_\gamma \rangle = 2.0$; then we have $\theta_\gamma \sim 37.^{\circ}5$ and $f_\gamma \sim 0.67$. After the position, period, magnetic field strength, and luminosity have been determined and the pulsar has been accepted according to the criteria mentioned above, we need to consider the detectability of the pulsar, namely, we determine whether the pulsar will be detectable at both radio and $\gamma$-ray energies. Therefore, the radio and $\gamma$-ray selection effects must be considered. For the radio selection effects, the minimum detectable average flux density, $S_{\rm min}$, of a pulsar's radio survey can be estimated by (e.g., Biggs & Lyne 1992; Sturner & Dermer 1996)

$$S_{\rm min} = \beta S_0 \left[\frac{T_{\rm rec} + T_{\rm sky}(l, b)}{T_0}\right]\left(\frac{W}{P - W}\right)^{1/2}, \quad (33)$$

where $\beta S_0$ is the flux limit when pulse broadening and background emission is negligible, $T_{\rm rec}$ is the receiver temperature, $T_{\rm sky}$ is the sky temperature at the survey frequency, $T_0$ is a normalization temperature, $P$ is the pulsar rotation period, and $W$ is the broadened radio-pulse width. $\beta S_0$, $T_{\rm rec}$, and $T_0$ are radio receiver parameters, which are 3.32 mJy, 20 K, and 45 K for the Parkes 1520 MHz receiver ($\nu = 1520$ MHz is the observing frequency, and $\delta\nu = 5.0$ MHz is the channel bandwidth) and 2.46 mJy, 10 K, and 90 K for the Arecibo 430 MHz receiver ($\nu = 430$ MHz and $\delta\nu = 0.25$ MHz). $T_{\rm sky}$ is given by (Johnston et al. 1992; Sturner & Dermer 1996)

$$T_{\rm sky}(\nu) = 25 + \left\{\frac{275}{[1 + (l/42)^2][1 + (b/3)^2]}\right\}\left(\frac{408\ {\rm MHz}}{\nu}\right)^{2.6}, \quad (34)$$

where $l$ and $b$ are the Galactic longitude and latitude, respectively. The broadened pulse width is given by

$$W^2 = W_0^2 + (\beta_1 \tau_{\rm samp})^2 + \tau_{\rm DM}^2 + \tau_{\rm scat}^2, \quad (35)$$

where $W_0 \approx 0.1P$ is the intrinsic radio pulse width; $\beta_1 = 2$; $\tau_{\rm samp}$ is the receiver sampling time, which is 1.2 ms for the Parkes receiver and 0.25 ms for the Arecibo receiver; $\tau_{\rm DM}$ is the frequency dispersion of the radio pulse as it passes through the interstellar medium and is given by

$$\tau_{\rm DM} = \left(\frac{\rm DM}{\rm DM_0}\right)\tau_{\rm samp}, \quad (36)$$

where ${\rm DM_0} = \tau_{\rm samp}\nu^3/8299\,\delta\nu$ pc cm$^{-3}$; DM is the dispersion measure of the pulsar; $\tau_{\rm scat}$ represents the broadening of the radio pulse due to scattering of the pulse and the subsequent path-length differences experienced by the observed photons and can be estimated by (Johnston et al. 1992; Sturner & Dermer 1996)

$$\tau_{\rm scat}(\nu) = \tau_{\rm scat,400}\left(\frac{400\ {\rm MHz}}{\nu}\right)^{4.4} \quad (37)$$

with $\tau_{\rm scat,400} = 10^{-4.61 + 1.14\log {\rm DM}} + 10^{-9.22 + 4.46\log {\rm DM}}$. The dispersion measure of the pulsar is calculated by using ${\rm DM} = \int n_e(R, Z)ds$, where the electron density is given by (Lyne, Manchester, & Taylor 1985; Bhattacharya et al. 1992; Sturner & Dermer 1996)

$$n_e(R, z) = \frac{1}{1 + R/R_0}\left(n_1 e^{-|z|/H_1} + n_2 e^{-|z|/H_2}\right), \quad (38)$$

where $R_0 = 8.0$ kpc is the Galactocentric radius of the Sun, $n_1 = 0.0188$ cm$^{-3}$, $H_1 = 70$ pc, $n_2 = 0.0313$ cm$^{-3}$, and $H_2 = 639$ pc. Furthermore, we use the assumption of Sturner & Dermer that the Arecibo receiver covers the Galactic plane with $30^{\circ} < l < 75^{\circ}$ and $|b| < 5^{\circ}$, and the rest of the sky is covered by the Parkes receiver. Therefore, from the above equations, we can estimate $S_{\rm min}$ for each pulsar at either 1520 or 430 MHz. Then we convert $S_{\rm min}$ at 1520 or 430 MHz into that at 400 MHz by assuming a power-law energy spectrum with spectral index of $-2$ for the pulsar radio emission (Biggs & Lyne 1992) and compare it with the model pulsar flux at 400 MHz. Those pulsars which satisfy

$$L_{400}/d^2 \geq S_{\rm min} \quad (39)$$

and

$$W < P \quad (40)$$

are considered to be radio-detectable pulsars, where $d$ is the distance to the pulsar. Now we consider the $\gamma$-ray selection effect. In our model, the luminosity of $\gamma$-rays with $E_\gamma > 100$ MeV can be approximated by equation (18). The corresponding energy flux can be written as

$$S_\gamma(>100\ {\rm MeV}) = \frac{L_\gamma(>100\ {\rm MeV})}{\Delta\Omega_\gamma\, d^2}, \quad (41)$$

For the $\gamma$-ray detection, Yadigaroglu & Romani (1995) used the value $S'_{\gamma,\rm min} = 3.0 \times 10^{-10}$ ergs cm$^{-2}$ s$^{-1}$, which can compare to the faintest 5 $\sigma$ sources in the first EGRET Galactic plane source catalog (Fichtel et al. 1994), but Sturner & Dermer (1996) adopted $2 \times 10^{-10}$ ergs cm$^{-2}$ s$^{-1}$. In this paper, we will use the value suggested by Yadigaroglu & Romani (1995). The pulsars which satisfy

$$S_\gamma(>100\ {\rm MeV})\Delta\Omega_\gamma \geq 3 \times 10^{-10}\ {\rm ergs\ cm^{-2}\ s^{-1}} \quad (42)$$

will be detectable as $\gamma$-ray pulsars.

### 3.2. *Monte Carlo Simulations*

After the initial properties of pulsars at birth are given, we can follow the luminosity and spatial evolution of the Galactic pulsar population by means of Monte Carlo simulations. The aim of these simulations is to produce the distributions of distance, period, age, magnetic field, and $\gamma$-ray flux of the $\gamma$-ray pulsars. Our simulations can be described by a number of sequential steps.

1. Generate pulsars with random ages less than $1 \times 10^6$ yr, which minimizes computing time.

2. Generate the initial position of a pulsar as random deviates with the probability density functions $\rho_z(z)$ and $\rho_R(R)$ given by equations (20) and (21).

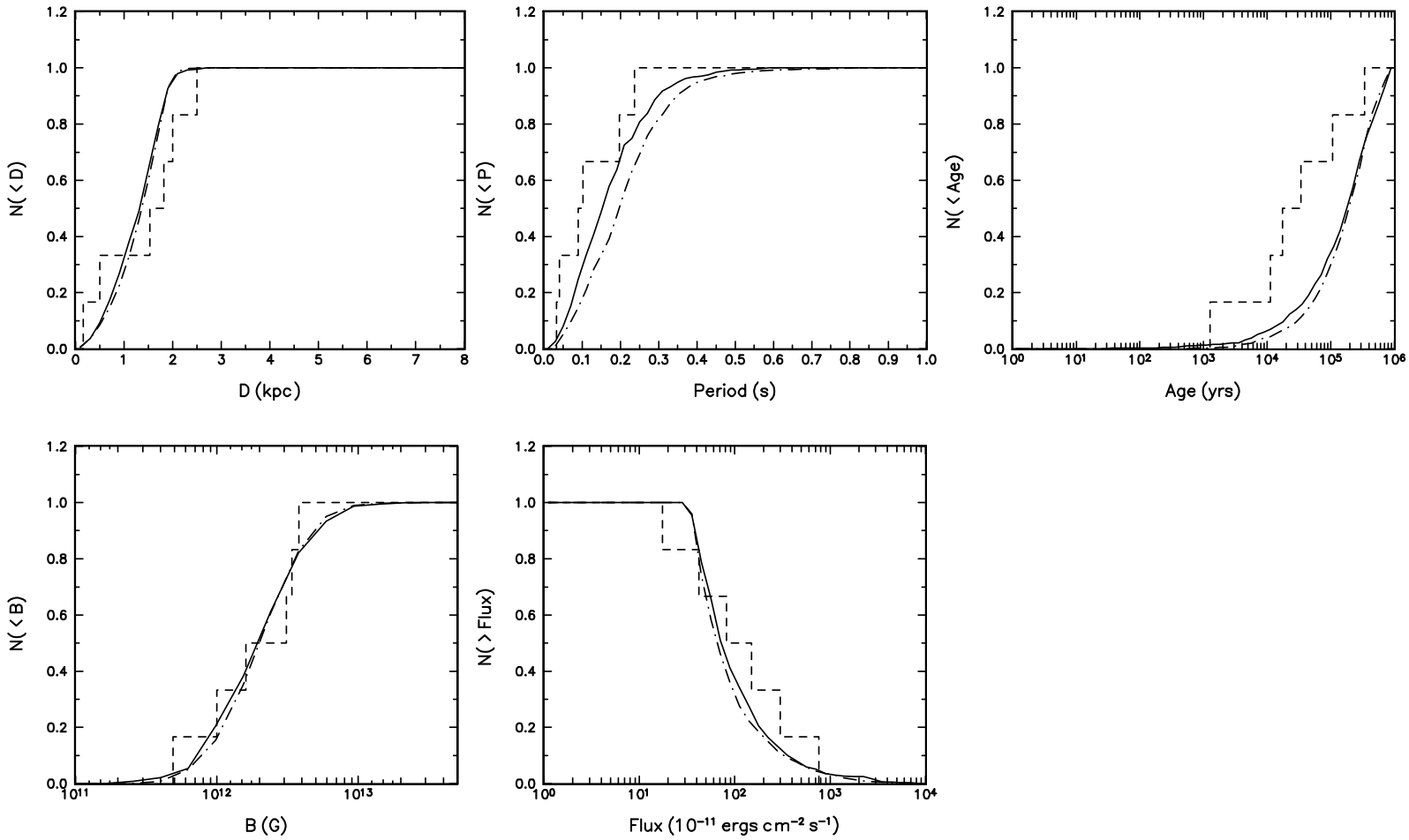


FIG. 2.—Normalized cumulative distributions of distance, period, age, magnetic field, and $\gamma$-ray energy flux of Galactic high-energy ($>100$ MeV) $\gamma$-ray pulsar population for our model with radio flux selection effects (*solid curves*) and without radio selection effects (*dot-dashed curves*). For comparison, corresponding distributions of the six observed $\gamma$-ray pulsars by EGRET are also shown (*dashed histograms*).

3. Generate the magnetic field of the pulsar with a random Gaussian deviate with probability density function described by equation (26).

4. Calculate the initial velocity of the pulsar, in which the random velocity is created as a random deviate with probability density function given by equation (25) and the circular velocity is determined by equation (22). The initial space velocity of a pulsar is the vector sum of the random velocity and circular velocity.

5. Calculate the pulsar period at time $t$ by using equation (30) and determine the position at time $t$ by following the pulsar's motion in the Galactic gravitational potential for a given initial position ($R$, $z$) (step 2) and initial velocity ($v_R$, $v_\phi$, $v_z$) (step 4).

6. Calculate the Galactic longitude and latitude by using equations (27) and (28), and the distance to the pulsar by using equation (29).

7. Calculate the radio beaming fraction given by equation (32) and generate a sample pulsar of period $P$ in one out of $f_r(P)^{-1}$ cases by using the Monte Carlo method. Then, generate the radio luminosity at 400 MHz as a random deviate with probability density function given by equation (31) and calculate the minimum radio energy flux given by equation (33) and broadened pulse width given by equation (35). Those pulsars which satisfy equations (39) and (40) are considered to be radio-detectable pulsars.

8. Calculate the $\gamma$-ray luminosity with $E_\gamma > 100$ MeV and compare it with the flux threshold. Those pulsars which satisfy equation (42) are considered to be both radio- and $\gamma$-ray–detectable pulsars. All the relevant information is recorded.

9. The $\gamma$-ray beaming factor, $f_\gamma \sim 0.67$, obtained by comparing with known $\gamma$-ray pulsars, is used. Since in the outer gap model the $\gamma$-ray beam and radio beam are not correlated in general, these two beaming fractions will be used independently.

Following the procedure described above, we perform Monte Carlo simulations of $10^6$ pulsars born during the past million years. Of course, we need to normalize to either the pulsar birthrate of $\sim 10^{-2}$ yr$^{-1}$ or the observed number of radio pulsars. We choose an initial period $P_0 = 10$ ms or 30 ms to perform our simulations. Furthermore, we consider two kinds of pulsars: one consists of the pulsars that satisfy both radio selection and $\gamma$-ray selection effects; the other consists of the pulsars for which only the $\gamma$-ray selection effect is taken into account. Therefore, radio-quiet $\gamma$-ray pulsars can be estimated. In Figure 2 the normalized cumulative distributions of distance, period, age, magnetic field, and $\gamma$-ray energy flux of the pulsars with an initial period of 30 ms in our model are shown (*solid curves*). Model distributions without taking the radio-flux selection effects into account are also given (*dot-dashed curves*). For comparison, the corresponding observed distributions for six known $\gamma$-ray pulsars (see Table 1) are shown. It should be noted that the $\gamma$-ray pulsar PSR B1509$-$58 and the possible $\gamma$-ray pulsar PSR B0656+14 have not been included because the former has not been detected in the energy range $E_\gamma > 100$ MeV and the latter has not been confirmed. Generally, the inclusion of the radio detection criterion preferentially eliminates the distant, long-period, and dim pulsars. In our model, however, the pulsars with $f \leq 1$ are considered to be $\gamma$-ray pulsars which emit high-energy $\gamma$-rays. From equation (3), this condition excludes the pulsars with longer period if their magnetic fields are within $10^{12}$–$10^{13}$ G. Therefore, the radio selection effects in our model are less important than those predicted by Sturner & Dermer (1996). We have also simulated the normalized cumulative distributions of the pulsars with $P_0 =$ 10 ms. There is only a negligible difference between their period distributions. In subsequent simulations, we will only use $P_0 = 30$ ms. We performed a Kolmogorov-Smirnov (KS) test to compare the cumulative model distributions with the distributions for the six EGRET pulsars. One-sample KS statistics is used, since the model samples have more than 150 pulsars. The hypothesis that model and observed pulsars were drawn from the same parent population can be rejected at better than the 80% level if the maximum deviation between the distributions is greater than 0.41. In our model, the maximum deviations of distance, period, age, magnetic field, and flux distributions from the observed distributions are 0.30, 0.37, 0.50, 0.20, and 0.22, respectively. It can be seen that four out of five of the cumulative distributions cannot be rejected at better than the 80% confidence level, and the fifth cannot be rejected at better than the 95% confidence level. Sturner & Dermer (1996) examined their model using the KS test. In their model 4X-P30, which best fitted the observed data (seven pulsars were used for the distance, period, age, and magnetic field distributions but six pulsars for the flux distribution), the corresponding maximum deviations for the five parameters are 0.20, 0.39, 0.25, 0.35, and 0.40, respectively. In our model, for the cumulative distance distribution, the model results predict a larger number of $\gamma$-ray pulsars between 1 and 2 kpc. The discrepancies between the model results and observed data can be understood by considering uncertainties of the observed distances for the six known $\gamma$-ray pulsars (at least 25% uncertainty for each pulsar). Furthermore, our model distributions of period, age, magnetic field, and energy flux will become more consistent with the data if more $\gamma$-ray pulsar candidates are confirmed. In fact, based on the analysis of the EGRET data in the vicinity of 14 radio-bright ($>1$ Jy at 1 GHz) supernova remnants, Esposito et al. (1996) suggested that the $\gamma$-ray emission near W44 may be due to the pulsar PSR B1853$-$01.

Finally, we would like to estimate the number of possible $\gamma$-ray pulsars from our statistical analysis. We find that the ratio of the $\gamma$-ray pulsars to radio pulsars from our samples is about 0.16, i.e., there are about 16 $\gamma$-ray pulsars in 100 radio pulsars. At present, 706 radio pulsars have been observed, but the ages of only 540 radio pulsars have been determined, and 105 radio pulsars have ages less than $10^6$ yr. Therefore, we have about 11 $\gamma$-ray pulsars that are also radio pulsars, where the $\gamma$-ray beaming fraction (0.67) is used. So we expect that about 11 high-energy $\gamma$-ray pulsars can be found out of $\sim 100$ detected radio pulsars with age less than $10^6$ yr.

## 4. GEMINGA-LIKE PULSARS AND UNIDENTIFIED POINT SOURCES OF EGRET

In this section, we consider the properties of Geminga-like pulsars. The Geminga-like pulsars are either those pulsars whose radio fluxes are lower than the radio survey flux threshold or those whose radio beams miss us. Hence, the constraints for the Geminga-like pulsars are (1) $f \leq 1$ and (2) $S_\gamma \geq 3 \times 10^{-10}$ ergs cm$^{-2}$ s$^{-1}$. We obtain the sample of the Geminga-like pulsars by means of the Monte

Carlo method as follows. First, we follow steps 1–6 of our simulation method outlined in § 3.2. Next, prior to step 7, step 8 is performed to generate the sample of $\gamma$-ray pulsars. In this sample (the number of pulsars is labeled as $N_{\gamma 1}$), some of the pulsars may satisfy the radio survey flux threshold. Hence, step 7 is performed to generate those pulsars which are detectable at both radio and $\gamma$-ray energies, where the number of these pulsars is represented by $N_{\gamma 2}$. Therefore, the number of the Geminga-like pulsars can be approximated by $(N_{\gamma 1} - N_{\gamma 2})$. Using the method mentioned above, we can obtain a Geminga-like pulsar sample and analyze the properties of the pulsars statistically. In Figure 3 we show the normalized distributions of distance, period, magnetic field, age, and the size of the outer gap, $f$, of the Geminga-like pulsars. It can be seen that the Geminga-like pulsars are distributed mainly in the distance region

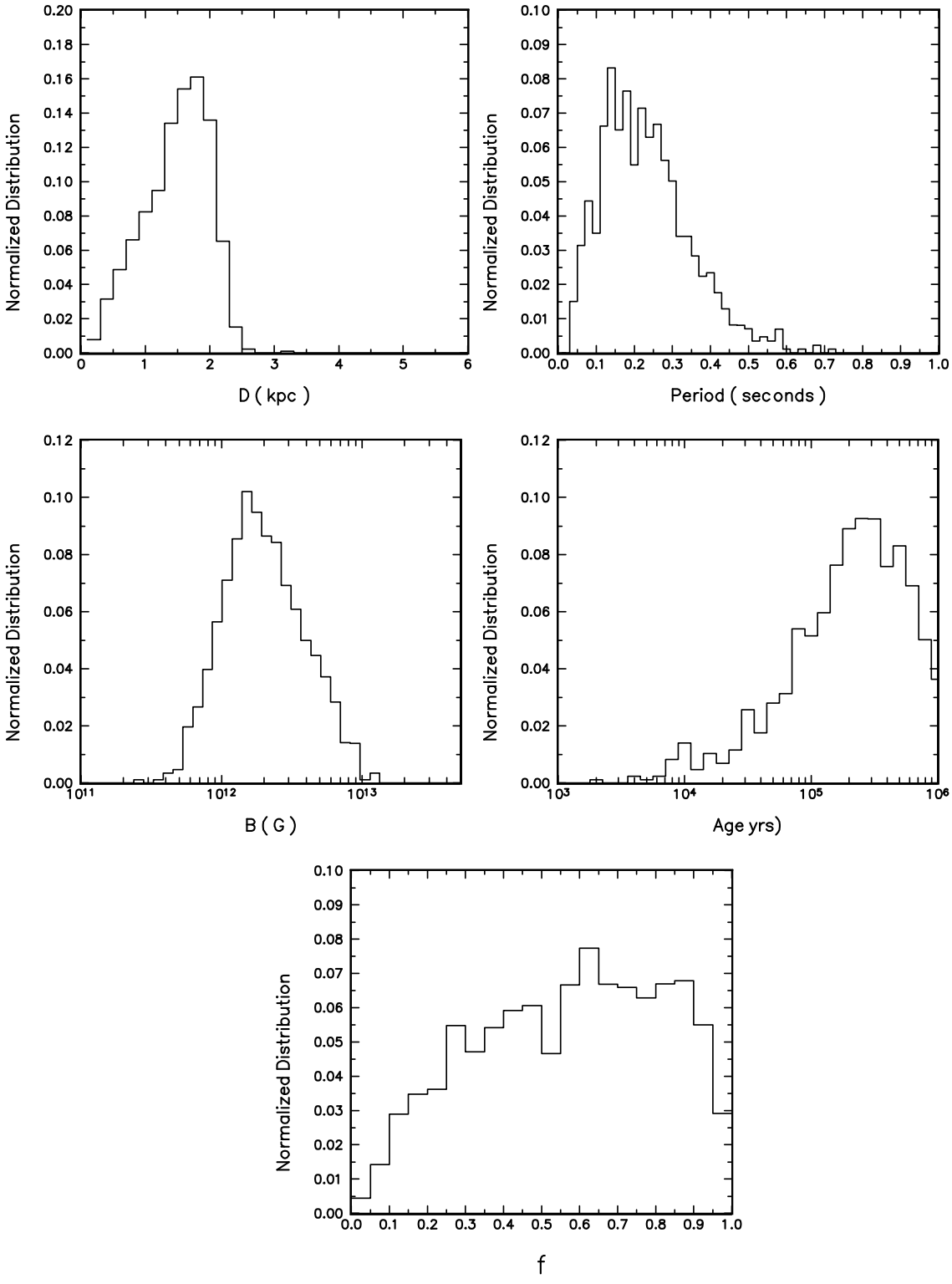


FIG. 3.—Normalized distributions of distance, period, magnetic field, age, and the outer gap size of Geminga-like pulsars

from 1 to 2 kpc, and most of the Geminga-like pulsars have periods between $\sim 0.1$ and 0.3 s, with magnetic fields from $\sim 8 \times 10^{11}$ to $\sim 5 \times 10^{12}$ G, ages between $10^5$ and $10^6$ yr, and the size of the outer gap from 0.3 to 0.9. In fact, from these simulated distributions, we should perhaps not be surprised that the Geminga is the first Geminga-like pulsar detected. Except for distance, the other parameters—the period ($P = 0.237$ s), the magnetic field ($B_{12} = 1.6$), and the age ($\tau = 3.4 \times 10^5$ yr) of the Geminga—are coincident with the peak positions of the distributions. So it is the most typical Geminga-like pulsar. But its distance is only $\sim 200$ pc, so that is why we find it first. Next we consider the high-energy $\gamma$-ray flux distribution from these pulsars. At present, EGRET has observed 96 unidentified point sources (Thompson et al. 1995, 1996). Kaaret & Cottam (1996) analyzed the unidentified EGRET sources at $|b| < 5°$ and found significant correlation between the positions of the unidentified EGRET sources and OB associations. They estimated distances to the unidentified EGRET sources from the OB associations and luminosities, and verified that the distribution of luminosities for the unidentified EGRET sources is consistent with that of known $\gamma$-ray pulsars. Therefore, Kaaret & Cottam concluded that a majority of the unidentified EGRET sources may be pulsars. Furthermore, based on their outer gap model, Yadigaroglu & Romani (1997) found that the spatial distribution and luminosities of the unidentified EGRET sources are consistent with the proposition that essentially all Galactic unidentified EGRET sources are pulsars. Whether or not these point sources are $\gamma$-ray pulsars has not yet been confirmed, although these data can be used as a possible test for our model predictions. In Figure 4 the comparisons of our model results with the distributions of high-energy ($>100$ MeV) $\gamma$-rays from these unidentified point sources at different latitude regions are shown. Our result indicates that the fluxes of Geminga-like pulsars at $|b| < 5°$ are concentrated mainly in the range from $\sim 3 \times 10^{-7}$ to $\sim 3 \times 10^{-6}$ cm$^{-2}$ s$^{-1}$, which is consistent with the observed data of 30 unidentified point sources detected by EGRET at $|b| < 5°$. Compared to the fluxes of all unidentified point sources, there are some difference between our model result and the observed data. This indicates that only some of the unidentified point sources at $|b| \geq 5°$ are Geminga-like pulsars. Furthermore, we can compare the Galactic distributions in $l$ and $b$ of the unidentified EGRET sources and modeled Geminga-like pulsars at $|b| < 5°$. From our statistical analysis, the number of Geminga-like pulsars is $\sim 55\dot{N}_{100}$, where $\dot{N}_{100}$ is the birthrate of neutron stars in units of 100 yr. Considering the beaming effect of $\gamma$-ray pulsars ($f_\gamma \sim 0.67$), the number of Geminga-like pulsars is $\sim 37\dot{N}_{100}$ in our Galaxy. In Figure 5 we show the comparison of the observed normalized distributions with the modeled results. For the longitude distribution, we divide the longitude into 18 bins. Assuming the observed unidentified EGRET sources and model pulsars in each bin are $N_i$ and $n_i$, then we have $\chi^2/\nu \approx 0.84$ using $\chi^2 = \sum_i (N_i - n_i)^2/n_i$, where $\nu$ is the number of degrees of freedom. For the latitude distribution (each bin width is 2°), we have $\chi^2/\nu \approx 1.42$ at $|b| < 5°$. Therefore, the model results are consistent with the observed distributions in both $l$ and $b$. Now we would like to describe how to discriminate the Geminga-like pulsars from other point sources. We have shown the properties of Geminga-like pulsars in Figure 3. Using these simulation results and the constraints men-

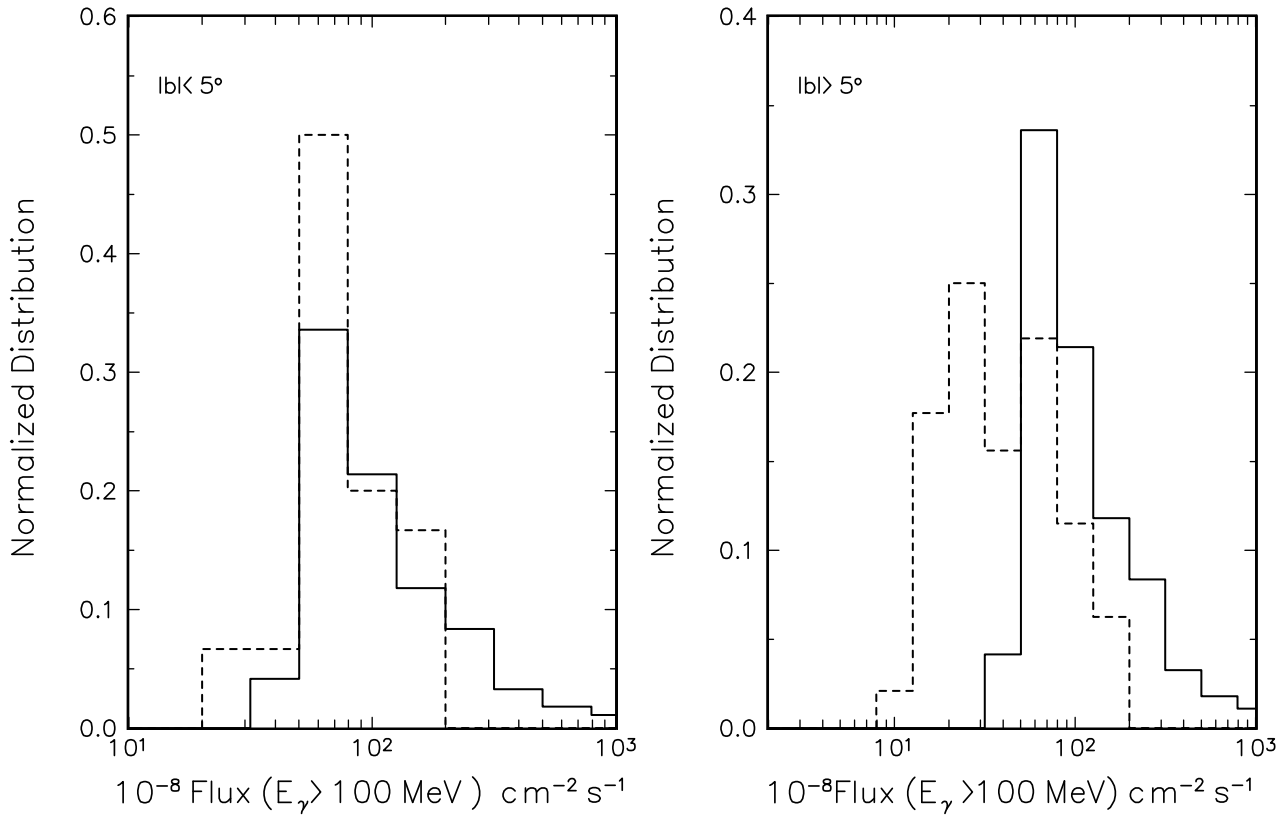


FIG. 4.—Comparison of the flux distribution of Geminga-like pulsars with that of the unidentified point sources detected by EGRET (Thompson et al. 1995, 1996), where model results are indicated by solid histograms and observed data are represented by dashed histograms.

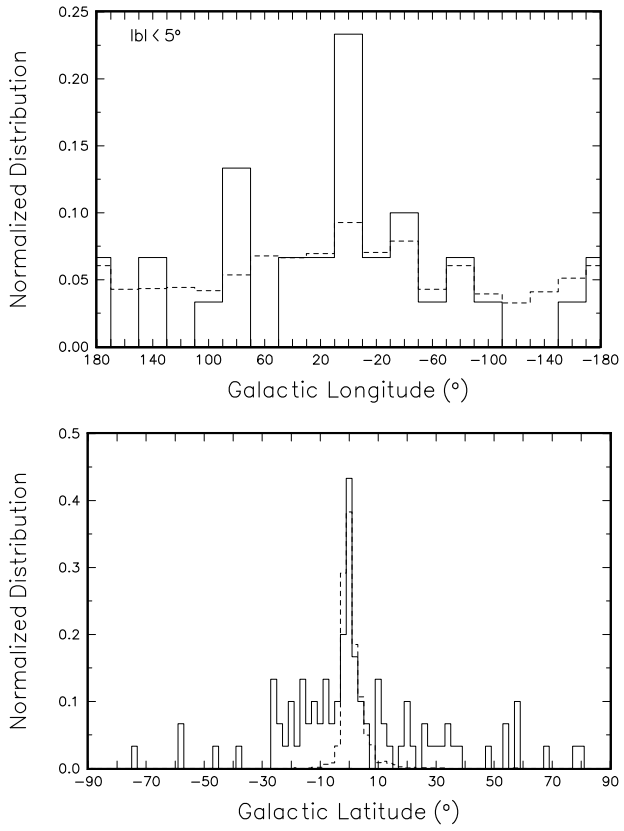


FIG. 5.—Normalized distributions of the Geminga-like pulsars in Galactic longitude $l$ and latitude $b$. The distributions of unidentified EGRET sources at $|b| < 5°$ are represented by the solid histograms, and those of the modeled Geminga-like pulsars are represented by dashed histograms.

tioned above, we propose to deduce the parameter range for the Geminga-like pulsars. In Figure 6 the contour in the *P-B* plane is shown, where the contour lines from inner to outer represent about 23%, 47%, 70%, and 95% probabilities, respectively. From this figure it can be seen that the parameter range of period and magnetic field for the Geminga-like pulsars is located in the area in which the period varies from $\sim 0.1$ to $\sim 0.3$ s and the magnetic field from $\sim 8 \times 10^{11}$ to $\sim 5 \times 10^{12}$ G in $\sim 70\%$ probability. In the next section we will use this parameter range. As mentioned above, based on the argument that EGRET source positions are related with SNRs and OB associations, Kaaret & Cottam (1996) and Yadigaroglu & Romani (1997) have estimated the distances of some EGRET unidentified point sources and concluded that young pulsars can account for essentially all of the excess low-latitude EGRET sources. Moreover, the spectra of some EGRET unidentified point sources have been obtained (Fierro 1995). Here we assume that these unidentified point sources are Geminga-like pulsars. We compare the cumulative model distance distribution with the distribution for both Geminga and the 12 unidentified sources given by Kaaret & Cottam (1996) in Figure 7. The KS test indicates that the maximum deviation from the observed is about 0.280. Because the hypothesis that the model pulsars and the observed unidentified sources were drawn from the same parent population can be rejected at greater than the 80% confidence level if the distribution is greater than 0.285, so the cumulative distribution cannot be rejected at this level. It should be pointed out that our model distance distribution is not consistent with the distribution estimated by Yadigaroglu & Romani (1997). Therefore, we use the parameter range of Geminga-like pulsars given above and the distances obtained by Kaaret & Cottam (1996) to calculate the spectra of five unidentified point sources that lie in $|b| \leq 5°$, and their distances are less than 2 kpc. We choose different values of period and magnetic field from the parameter range shown in Figure 6 and calculate the spectra by using the consistent fitting parameters and the distances for each unidentified point source. Finally, the values of period and magnetic field are determined by com-

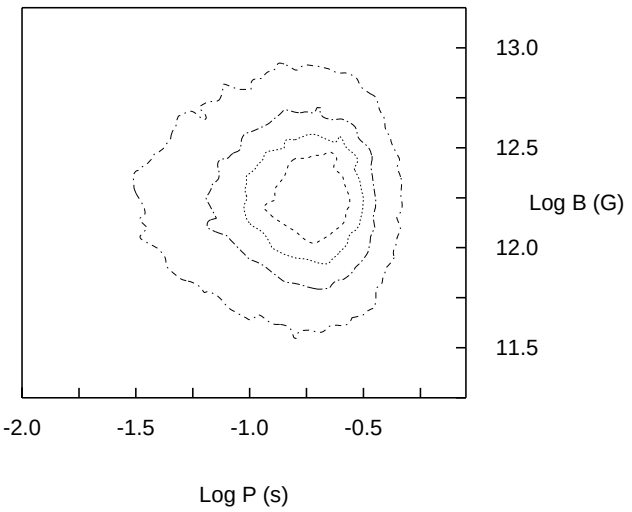


FIG. 6.—Magnetic field strength vs. period for the sample of Geminga-like pulsars (see text for details). The contour lines from inner to outer represent about 23%, 47%, 70%, and 95% probabilities.

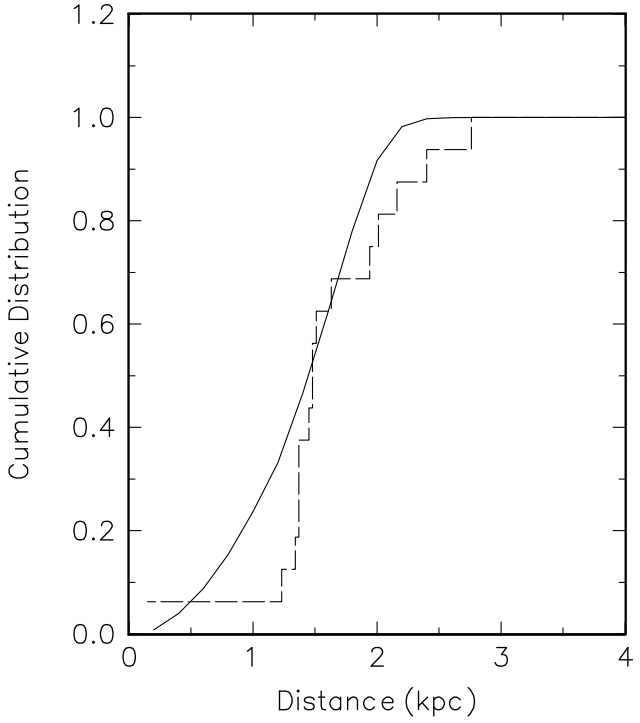


FIG. 7.—Comparison of the cumulative model distance distribution for Geminga-like pulsars with that for both Geminga and the 12 unidentified sources given by Kaaret & Cottam (1996).

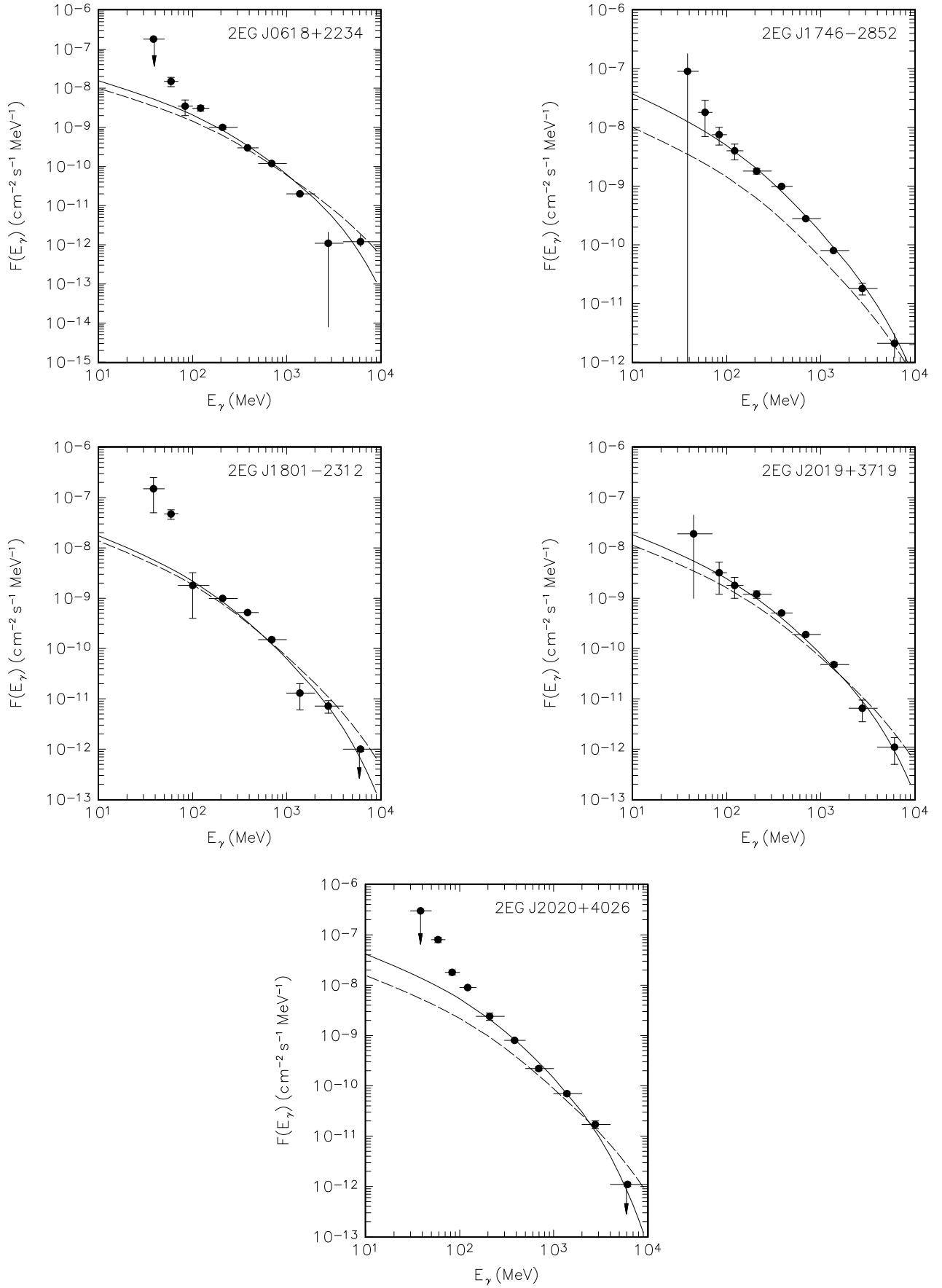


FIG. 8.—Comparison of our model results with observed spectra for five EGRET unidentified point sources, where dashed curves represent our results with consistent-fit parameters and solid curves represent our results with best-fit parameters.

TABLE 2

BEST-FIT MODEL PARAMETERS AND EXPECTED X-RAY LUMINOSITIES OF FIVE UNIDENTIFIED POINT SOURCES

| Name | $P$ (s) | $B_{12}$ (G) | $d$ (kpc) | $x_{\min}$ | $x_{\max}$ | $\Delta\Omega_\gamma$ | $T_{s6}$[a] | log $L_X^{soft}$[b] | log $L_X^{syn}$[b] |
|---|---|---|---|---|---|---|---|---|---|
| 2EG J0618+2234..... | 0.1 | 0.8 | 1.34 | 0.72 | 2.1 | 1.4 | 0.72 | 32.28 | 30.81 |
| 2EG J1746-2852 ..... | 0.3 | 5.0 | 1.50 | 0.68 | 2.1 | 0.6 | 0.78 | 32.41 | 30.28 |
| 2EG J2020+4026..... | 0.3 | 5.0 | 1.37 | 0.80 | 2.1 | 0.9 | 0.78 | 32.41 | 30.28 |
| 2EG J2019+3719..... | 0.2 | 2.0 | 1.37 | 0.72 | 2.1 | 1.2 | 0.74 | 32.32 | 30.30 |
| 2EG J1801−2312..... | 0.1 | 5.0 | 1.44 | 0.70 | 2.1 | 1.8 | 0.88 | 32.61 | 32.61 |

[a] $T_{s6} = T_s/10^6$.
[b] $L_X^{soft}$ and $L_X^{syn}$ are in units of ergs s$^{-1}$.

paring model results with the observed data. In Figure 8 the comparisons of our results with observed spectra for five EGRET unidentified point sources are shown, where dashed curves represent the results with consistent-fit parameters and solid curves represent the results with best-fit parameters shown in Table 2. In Table 2 the expected X-ray luminosities are also given for these sources. In order to account for the fact that our consistent-fit parameters produce spectra that are consistent with the observed spectra, we estimated the $\chi^2$ values for the best-fit versus consistent-fit parameters for each pulsar. For each pulsar, the fluxes for the consistent-fit and best-fit parameters at the observed energy bands are calculated. The $\chi^2$ values for 2EG J0618+2234, 2EG J1746−2852, 2EG J1801−2312, 2EG J2019+3719, and 2EG J2020+4026 are 2.9, 3.7, 1.6, 2.2, and 3.0, respectively. It can be seen that our results are consistent with the observed spectra. Therefore, these sources may be Geminga-like pulsars, especially 2EG J2019+3719.

## 5. POSSIBLE GAMMA-RAY PULSARS

In our Monte Carlo simulations, we predict that there should be 11 pulsars which can be detected in both radio and $\gamma$-ray energy bands. Six radio pulsars have already been identified as EGRET sources. In this section we attempt to determine which radio pulsars should be the most possible $\gamma$-ray pulsars. Generally, the EGRET threshold for point source detection above 100 MeV cannot be lower than $F_{\min} \geq 10^{-7}$ photons cm$^{-2}$ s$^{-1}$. However, the actual threshold depends on the local $\gamma$-ray background and instrument exposure and accuracy of pulsar parameters. Moreover, the minimum pulsed flux with $E_\gamma \geq 100$ MeV from known $\gamma$-ray pulsars detected by EGRET is that from PSR B1951+32, which is $(1.6 \pm 0.2) \times 10^{-7}$ cm$^{-2}$ s$^{-1}$ (Ramanamurthy et al. 1995). Here we will use the flux as threshold flux for detecting a pulsar as a point source in the EGRET range. Based on the data analysis, Fierro (1995) pointed out that the strongest candidates for $\gamma$-ray emission from radio pulsars are binary millisecond pulsars PSR J0034−0534 and J0613−0200, and the young pulsars PSR B1046−58, B1832−06, and B1853+01. Here we would like to present some predictions of our model. We use the database of radio pulsars provided by Princeton University, where the parameters of a total of 706 pulsars are given. From this database, we select 52 canonical pulsars that satisfy the condition of $f \leq 1$. We divide these pulsars into two groups based on their Galactic latitudes: one is the Galactic plane group with $|b| \leq 10°$, and the other is the non–Galactic plane group with $|b| > 10°$. In general, the local $\gamma$-ray background at high latitude is lower than that in the Galactic plane, compared to that at low latitude if they have same fluxes, so the $\gamma$-ray from the pulsar at high latitude can be easier to detect.

We have estimated the $\gamma$-ray flux with $E_\gamma > 100$ MeV by using the parameters of 52 canonical pulsars. We assume that the average solid angle is 2 sr. The results are shown in Figure 9, where the fluxes from six $\gamma$-ray pulsars are represented by filled circles; the open circles and filled diamonds represent the pulsars with $F_\gamma(E_\gamma > 100 \text{ MeV}) \geq 1.6 \times 10^{-7}$ cm$^{-2}$ s$^{-1}$ and $F_\gamma(E_\gamma > 100 \text{ MeV}) < 1.6 \times 10^{-7}$ cm$^{-2}$ s$^{-1}$ of the Galactic plane group, respectively. The empty box represents the pulsar located out of the Galactic plane, while plus signs represent the pulsars with X-ray emission. It can be seen that there are 14 canonical pulsars with $F_\gamma(E_\gamma > 100 \text{ MeV}) \geq 1.6 \times 10^{-7}$ cm$^{-2}$ s$^{-1}$ (including six known $\gamma$-ray pulsars). This number is very close to our Monte Carlo results. According to our model, each of these pulsars has 67% probability of being detected as a $\gamma$-ray pulsar. It should be pointed out that in our model there are six pulsars whose fluxes are between $10^{-7}$ and $1.6 \times 10^{-7}$ cm$^{-2}$ s$^{-1}$: PSR B1046−58, PSR B1221−63, PSR B1509−58, PSR B1719−37, PSR B1737−30, and PSR B1853+01. Based on the data analysis of EGRET, Fierro (1995) suggested that PSR B1509−58, B0656+14, B1046−58, and B1853+01 are the strongest candidates for $\gamma$-ray pulsars. He also pointed out that PSR B1823−13 and B1832−06 are possible candidates of $\gamma$-ray pulsars, but our model results give $F_\gamma(E_\gamma > 100 \text{ MeV}) \sim 7.4 \times 10^{-8}$ and $\sim 2.3 \times 10^{-8}$ cm$^{-2}$ s$^{-1}$ for these two pulsars, respectively. As to PSR B0656+14, our model result is greater than the

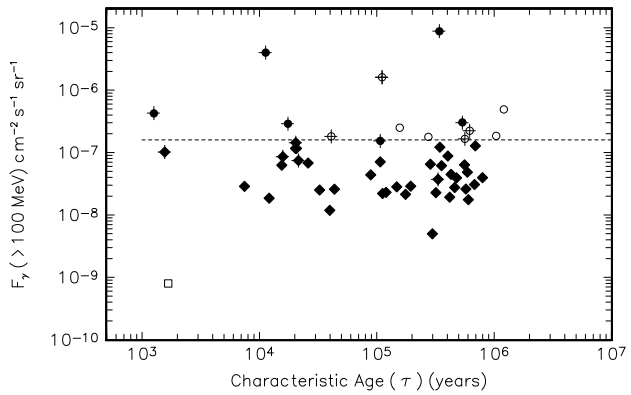


FIG. 9.—Predicted flux of high-energy ($E_\gamma > 100$ MeV) $\gamma$-rays from the pulsars as a function of pulsar characteristic age. Filled circles represent the six detected EGRET pulsars. Open circles and filled diamonds represent the pulsars with $F_\gamma(E_\gamma > 100 \text{ MeV}) \geq 1.6 \times 10^{-7}$ cm$^{-2}$ s$^{-1}$ and $F_\gamma(E_\gamma > 100 \text{ MeV}) < 1.6 \times 10^{-7}$ cm$^{-2}$ s$^{-1}$ within Galactic latitude $|b| \leq 10°$; open squares represent the pulsars in high Galactic latitude $|b| > 10°$, and plus signs represent pulsars with X-rays, where $\Delta\Omega_\gamma = 2.0$ sr is used.

TABLE 3

EXPECTED PULSARS WITH $F_\gamma(>100\ \mathrm{MeV}) > 1.6 \times 10^{-7}\ \mathrm{cm}^{-2}\ \mathrm{s}^{-1}$ IN OUR MODEL (EXCLUDING SIX KNOWN $\gamma$-RAY PULSARS)

| Pulsar | Age (yr) | $P$ (s) | $B_{12}$ (G) | $d$ (kpc) | $f$ | $F_\gamma(>100\ \mathrm{MeV})$ |
|---|---|---|---|---|---|---|
| B0114+58..... | 0.275E+06 | 0.101 | 0.780E+00 | 2.140 | 0.373 | 0.1778E−06 |
| B0355+54[a]..... | 0.564E+06 | 0.156 | 0.839E+00 | 2.070 | 0.611 | 0.1661E−06 |
| J0538+2817[a]..... | 0.619E+06 | 0.143 | 0.733E+00 | 1.770 | 0.592 | 0.2239E−06 |
| B0656+14[a]..... | 0.111E+06 | 0.385 | 0.466E+01 | 0.760 | 0.700 | 0.1608E−05 |
| B0740−28..... | 0.157E+06 | 0.167 | 0.169E+01 | 1.890 | 0.443 | 0.2505E−06 |
| B1449−64..... | 0.104E+07 | 0.179 | 0.711E+00 | 1.840 | 0.797 | 0.1849E−06 |
| J2043+2740 ..... | 0.121E+07 | 0.096 | 0.352E+00 | 1.130 | 0.550 | 0.4907E−06 |
| B2334+61[a]..... | 0.409E+05 | 0.495 | 0.986E+01 | 2.470 | 0.623 | 0.1821E−06 |

[a] Pulsars with X-rays (Becker & Trümper 1997).

upper limit by an order of magnitude and is about 39 times the value deduced by Ramanamurthy et al. (1996). In fact, the expected fluxes in other models are also greater than the observed data for this pulsar (Ramanamurthy et al. 1996). It is likely that we have missed the major $\gamma$-ray beam of PSR B0656+14. In Table 3 we show the model results for pulsars with $F_\gamma(>100\ \mathrm{MeV}) \geq 1.6 \times 10^{-7}\ \mathrm{cm}^{-2}\ \mathrm{s}^{-1}$. Therefore, adding the six known $\gamma$-ray pulsars, there are about 14 pulsars with high-energy ($>100$ MeV) $\gamma$-rays. Since in our outer gap model, X-rays and $\gamma$-rays are strongly correlated (cf. § 2), the strongest candidates of $\gamma$-ray pulsars may therefore be canonical pulsars with strong X-ray, e.g., PSR J0538+2817, PSR B0355+54, and PSR B2334+61. More specifically, we suggest that the signatures for $\gamma$-ray pulsars are (i) power-law behavior of the $\gamma$-ray spectrum with $\alpha_\gamma \sim -1.7$ to $-2.2$ from 100 MeV to a few GeV, (ii) power-law behavior of the hard X-ray spectrum with $\alpha_x \sim -2$ from keV to MeV, (iii) a soft thermal X-ray component with $kT \sim 10^2$ eV, and (iv) $L_X/\dot{E}_{sd} \sim 10^{-2}$–$10^{-3}$.

## 6. CONCLUSIONS

Using the six detected EGRET $\gamma$-ray pulsars and the database for $\gamma$-ray emission from all known spin-powered pulsars with $\dot{E}_{33}/d^2_{kpc} \geq 0.5$ given by Nel et al. (1996), we have tested the model and deduced a set of consistent-fit parameters which is very important (i) to predict the spectrum of unidentified $\gamma$-ray sources and not-yet-confirmed $\gamma$-ray pulsars and (ii) to carry out our statistical analysis of the $\gamma$-ray pulsars. Our results indicate that our model can successfully explain the $\gamma$-ray emission from spin-powered pulsars. Our model predicts that the conversion efficiency of high-energy $\gamma$-rays depends on the characteristic age and the period of pulsars, i.e., $\eta_{th} \propto \tau^{6/7} P^2$. Furthermore, we have also reviewed the X-ray emission from pulsars. This is not only important in calculating the size of the outer gap, which plays an important role in our statistical analysis, but also the X-ray properties of pulsars allow us to predict which EGRET sources and radio pulsars are likely $\gamma$-ray pulsars. Based on our model, the properties of the Galactic high-energy $\gamma$-ray pulsar population have been simulated by means of Monte Carlo methods. The initial magnetic field, spatial, and velocity distributions of the neutron star at birth (obtained by the radio pulsar statistical studies) have been used in our simulations, where the radio and $\gamma$-ray beaming fractions of the pulsars have been taken into account. We have modeled the distance, period, age, magnetic field, and high-energy ($>100$ MeV) $\gamma$-ray energy flux distributions of the Galactic $\gamma$-ray pulsar population and find them consistent with those of the six observed $\gamma$-ray pulsars by EGRET. From our statistical analysis, we expect that about 11 $\gamma$-ray pulsars whose fluxes are greater than the EGRET threshold, and which also are radio pulsars, may exist in our Galaxy. Furthermore, we have obtained the distributions of period, magnetic field, distance, age, and energy flux for the Geminga-like pulsars. Comparing the high-energy ($>100$ MeV) $\gamma$-ray flux and the Galactic distributions in Galactic longitude and latitude with those of unidentified EGRET point sources in the Galactic plane, we conclude that a majority of the unidentified EGRET point sources are probably Geminga-like pulsars. We have also predicted that there may be $\sim 55 f_\gamma \dot{N}_{100}$ in our Galaxy, where $f_\gamma$ is the beaming fraction of $\gamma$-ray pulsars, and we have used an average value (0.67) to estimate the number of the Geminga-like pulsars. Helfand (1994) pointed out that $0.2 \leq f_\gamma < 1$ (see Fig. 3 of his paper). By fitting the observed data of the six known $\gamma$-ray pulsars, we estimate that $f_\gamma \sim 0.67$. Furthermore, we have shown the possible range of parameters for the Geminga-like pulsars: their periods are mainly from 0.1 to 0.3 s, the magnetic fields are mainly from $8 \times 10^{11}$ to $5 \times 10^{12}$ G, and they must satisfy $B_{12} \geq 20 P^{2.2}$ G. Finally, we have estimated the high-energy $\gamma$-ray flux with $E_\gamma > 100$ MeV by using the database of 706 pulsars given by Princeton University, and we suggest that the strongest candidates of $\gamma$-ray pulsars may be canonical pulsars with strong X-ray emission satisfying $L_X/\dot{E}_{sd} \sim 10^{-3}$ (Cheng et al. 1998).

We thank T. Bulik, A. da Costa, J. Gil, D. R. Lorimer, G. Melikidze, and B. Rudak for useful discussion and suggestions. We are grateful to T. C. Boyce for a critical reading of our manuscript and the anonymous referee for his/her useful comments. This work is partially supported by a RGC grant of the Hong Kong Government.

REFERENCES

Bailes, M., & Kniffen, D. A. 1992, ApJ, 391, 659
Becker, W., & Trümper, J. 1997, A&A, in press
Bhattacharya, D., Wijers, R. A. M. J., Hartman, J. W., & Verbunt, F. 1992, A&A, 254, 198
Biggs, J. D. 1990, MNRAS, 245, 514
Biggs, J. D., & Lyne, A. G. 1992, MNRAS, 254, 257
Brazier, K. T. S., et al. 1994, MNRAS, 268, 517
Cheng, K. S., & Ding, W. K. Y. 1994, ApJ, 431, 724
Cheng, K. S., Gil, J., & Zhang, L. 1998, ApJ, in press
Cheng, K. S., Ho, C., & Ruderman, M. A. 1986a, ApJ, 300, 500 (CHR I)
———. 1986b, ApJ, 300, 522 (CHR II)
Cheng, K. S. & Wei, D. M. 1995, ApJ, 448, 281
Cheng, K. S., & Zhang, J. L. 1996, ApJ, 463, 271
Chiang, J., & Romani, R. W. 1992, ApJ, 400, 724
Dermer, C. D., & Sturner, S. J. 1994, ApJ, 420, L75
Emmering, R. T., & Chevalier, R. A. 1989, ApJ, 345, 931
Erber, T. 1966, Rev. Mod. Phys., 38, 626
Esposito, J. A., Hunter, S. D., Kanbach, G., & Sreekumar, P. 1996, ApJ, 461, 820
Fichtel, C. E., et al. 1994, ApJ, 434, 557
Fierro, J. M. 1995, Ph.D. thesis, Stanford Univ.
Fierro, J. M., et al. 1995, ApJ, 447, 807
Gil, J., & Han, J. L. 1996, ApJ, 458, 265
Gil, J., Kijak, J., & Seiradakis, J. H. 1993, A&A, 272, 268
Goldreich, P., & Julian, W. H. 1969, ApJ, 157, 869
Halpern, J. P., & Ruderman, M. A. 1993, ApJ, 415, 286
Harding, A. K. 1981, ApJ, 245, 267
Helfand, D. J. 1994, MNRAS, 267, 490
Ho, C. 1989, ApJ, 342, 369
Johnston, S., Lyne, A. G., Manchester, R. N., Kniffen, D. A., D'Amico, N., Lim, J., & Ashworth, M. 1992, MNRAS, 255, 401
Kaaret, P., & Cottam, J. 1996, ApJ, 462, L35
Lyne, A. G., & Lorimer, D. R. 1994, Nature, 369, 127
Lyne, A. G., & Manchester, R. N. 1988, MNRAS, 234, 477
Lyne, A. G., Manchester, R. N., & Taylor, J. H. 1985, MNRAS, 213, 613
Narayan, R., & Ostriker, J. P. 1990, ApJ, 352, 222
Narayan, R., & Vivekanand, M. 1983, ApJ, 274, 771
Nel, H. I., et al. 1996, ApJ, 465, 898
Paczyński, B. 1990, ApJ, 348, 485
Press, W., Flannery, B., Teukolsky, S., & Vetterling, W. 1992, Numerical Recipes: The Art of Scientific Computing (2d ed.; Cambridge: Cambridge Univ. Press)
Ramanamurthy, P. V., et al. 1995, ApJ, 447, L109
———. 1996, ApJ, 458, 755
Romani, R. W. 1996, ApJ, 470, 469
Rudak, B., & Dyks, J. 1997, MNRAS, in press
Ruderman, M. A., & Sutherland, P. 1975, ApJ, 196, 57
Sturner, S. J., & Dermer, C. D. 1996, ApJ, 461, 872
Taylor, J. H., Manchester, R. N., & Lyne, A. G. 1993, ApJS, 88, 529
Thompson, D. J., et al. 1994, ApJ, 436, 229
———. 1995, ApJS, 101, 259
———. 1996, ApJS, 107, 227
Vivekanand, M., & Narayan, R. 1981, A&A, 2, 315
Yadigaroglu, I. A., & Romani, R. W. 1995, ApJ, 372, L99
———. 1997, ApJ, 476, 347
Zhang, L., & Cheng, K. S. 1997, ApJ, 487, 370 (ZC97)
———. 1998, MNRAS, in press